

Optimal persistent currents for ultracold bosons stirred on a ring

Marco Cominotti,¹ Davide Rossini,² Matteo Rizzi,³ Frank Hekking,¹ and Anna Minguzzi¹

¹*Université Grenoble 1/CNRS, Laboratoire de Physique et de Modélisation des Milieux Condensés (UMR 5493), B.P. 166, 38042 Grenoble, France*

²*NEST, Scuola Normale Superiore and Istituto Nanoscienze-CNR, I-56126 Pisa, Italy*

³*Johannes-Gutenberg-Universität Mainz, Institut für Physik, Staudingerweg 7, D-55099 Mainz, Germany*

(Dated: May 19, 2022)

We study persistent currents for interacting bosons on a tight ring trap, subjected to an artificial gauge field induced by a rotating barrier potential. We show that at intermediate interactions the persistent current response is maximal, due to a subtle interplay of effects due to the barrier, the interaction and quantum fluctuations. These results are relevant for ongoing experiments with ultracold atomic gases on mesoscopic rings.

PACS numbers: 67.85.-d, 03.75.Lm, 71.10.Pm, 73.23.Ra

A quantum fluid confined on a ring subjected to an artificial gauge field is predicted to display a periodic behavior of the particle current as a function of the flux corresponding to the gauge field. This *persistent current* phenomenon, which is a manifestation of the Aharonov-Bohm effect, is a consequence of the macroscopic coherence of the many-body wavefunction along the entire ring.

Persistent currents have been first observed more than sixty years ago in bulk superconductors [1–3], where macroscopic coherence is naturally present, and, more recently, in normal metallic rings [4–7], where the observation has been challenging due to the decoherence induced by inelastic scattering. Recent advances of trapping and cooling of ultracold atoms on tight ring traps [8–16] have provided a novel system to explore persistent currents. The high-purity of the system, the tunability of the parameters and of the geometry are expected to allow an unprecedented test of the theory, as well as applications to high-precision measurements, atom interferometry, and quantum information.

In quasi-one-dimensional rings, persistent currents offer the possibility to explore fundamental properties, such as the interplay between interactions, quantum fluctuations and mesoscopic effects. Parity effects, *i.e.*, a diamagnetic or paramagnetic response of the persistent currents depending on the parity of the number of particles on the ring, are expected for fermions but not for bosons [17]. For the fermionic case, in the absence of any barrier or impurity along the ring, Leggett conjectured [18] that the system displays ideal persistent currents, namely, a perfect sawtooth behavior as a function of the flux for any interaction strength at zero temperature. This was subsequently confirmed by Loss [19] and by Müller-Groeling and collaborators [20]. It implies perfect superfluidity, according to its definition through the stiffness, *i.e.*, the response in the ground-state energy of the system to a twist of the boundary conditions [21] [22]. If a localized barrier is added, persistent currents are smeared—the persistent current shape taking a sinusoidal form in the

large-barrier or small-tunneling limit—as is well known for thin superconducting rings from a Luttinger-liquid approach [23, 24]. The details of this smearing strongly depend on the interaction strength. In ultracold atomic gases in a quasi-one-dimensional geometry, the interaction strength is tunable, allowing to experimentally reach both the regimes of weak and strong interactions, up to the impenetrable-boson limit [25, 26]. An open question, relevant for future experiments, is therefore the behavior of persistent currents in all interaction and barrier strength regimes. This is the purpose of the present work. To cover all interaction regimes, we take advantage of a combination of analytical as well as numerical approaches. On the one hand, we use Gross-Pitaevskii (GP) theory at weak interactions, the Luttinger-liquid (LL) model at intermediate interactions, and the Tonks-Girardeau (TG) solution in the strongly interacting impenetrable boson limit. On the other hand, we employ a numerical variational technique based on the matrix-product-state (MPS) representation of the system wavefunction. As a main result, by tuning the interparticle interaction strength at fixed barrier strength we find an optimum value of the current amplitude, which illustrates the non-trivial combination of interaction, quantum fluctuations and barrier effects.

Persistent currents for rotating bosons.— Let us consider a one-dimensional (1D) ring of circumference L , containing N bosons of mass M , at zero temperature, interacting with each other via a contact potential $v(x - x') = g\delta(x - x')$. The ring contains a localized barrier, modeled by the potential $U_b(x, t) = U_0\delta(x - Vt)$, that moves along its circumference at constant velocity V . This induces an effective Coriolis flux $\Omega = MVL/2\pi\hbar$ in the rotating frame. We are interested in the stationary regime, reached after the barrier has been adiabatically switched on at early times, such that no high-energy excitations are created. At zero temperature, the spatially-averaged particle current $I(\Omega)$ is obtained from the ground-state energy $E(\Omega)$ via the thermodynamic re-

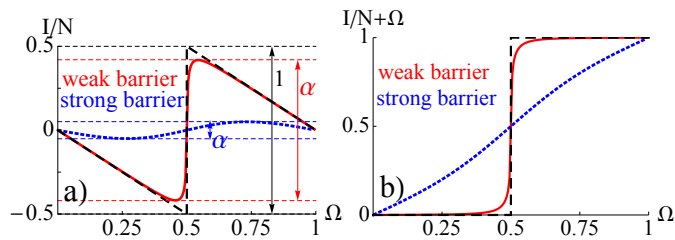


FIG. 1. (Color online) Integrated current per particle (a) in the rotating frame $I(\Omega)/N$ and (b) in the non-rotating frame $I(\Omega)/N + \Omega$, in units of $I_0 = 2\pi\hbar/ML$ for $N = 18$. In absence of the barrier the maximum attainable amplitude is $\alpha = 1$ in our units, corresponding to the perfect sawtooth and staircase in the two frames respectively (black-dashed line). At weak barrier strength ($\lambda = 0.2$, $\gamma = 0.004$), the current is a smeared sawtooth/staircase respectively (red-solid line) while at strong barrier strength ($\lambda = 10$, $\gamma = 0.004$) there is a crossover to a sinusoidal/modulated-linear behavior respectively (blue dotted line).

lation [27]

$$I(\Omega) = -\frac{1}{2\pi\hbar} \frac{\partial E(\Omega)}{\partial \Omega}. \quad (1)$$

In the absence of a barrier, for any interaction strength, the ground-state energy $E(\Omega)$ is a series of parabolas with well-defined angular momentum, shifted with respect to each other by Galilean translation [28]. The parabolas intersect at the so-called frustration points $\Omega_j = (2j+1)/2$. The corresponding particle current is then a perfect sawtooth in the rotating frame and a staircase in the non-rotating frame, corresponding to states with well-defined angular momentum in the system (dashed lines in Fig. 1). Introduction of a small barrier breaks the rotational invariance and mixes states of different angular momentum. The corresponding integrated current $I(\Omega)$ is a smeared sawtooth in the rotating frame and a smeared staircase in the non-rotating one (solid lines in Fig. 1). For large barrier strengths, the integrated current is a small-amplitude sinusoid in the rotating frame and a straight line with a small modulation in the non-rotating one (dotted lines in Fig. 1). In all regimes of barrier strength we characterize the integrated current profile as a function of the Coriolis flux using the amplitude α of the integrated current per particle $I(\Omega)/N$ in the rotating frame (see again Fig. 1). In the following we will determine α for all regimes of dimensionless interaction strengths $\gamma = Mg/\hbar^2 n_0$, with $n_0 = N/L$ and dimensionless barrier strength $\lambda = MU_0L/\pi\hbar^2$.

Exactly solvable points.—The system Hamiltonian in the co-rotating frame,

$$\mathcal{H} = \sum_{j=1}^N \frac{\hbar^2}{2M} \left(-i \frac{\partial}{\partial x_j} + \frac{2\pi\Omega}{L} \right)^2 + U_0 \delta(x_j) + \frac{g}{2} \sum_{j,l=1}^N \delta(x_l - x_j), \quad (2)$$

is a generalization of the Lieb-Liniger model [29] to the rotating case, and is non-integrable due to the presence of the barrier. Its eigenvalues are periodic in Ω with period 1.

In the two limiting cases of a non-interacting and an infinitely-interacting gas, it is possible to find an exact solution to the many-body Schrödinger equation $\mathcal{H}\Psi(x_1, \dots, x_N) = E\Psi(x_1, \dots, x_N)$. For a non-interacting Bose gas, the many-body wavefunction $\Psi_{\text{NI}}(x_1, \dots, x_N) = \prod_{i=1}^N \psi_0(x_i)$ is given by the product of N identical single-particle wavefunctions $\psi_0(x_i)$, which are ground-state solutions of the corresponding one-body Schrödinger equation, $\frac{\hbar^2}{2M} (-i\partial_x + \frac{2\pi}{L}\Omega)^2 \psi_n + U_0\delta(x)\psi_n = \varepsilon_n\psi_n$, and has energy $E_{\text{NI}} = N\varepsilon_0$. In the infinitely-interacting limit of impenetrable bosons, or TG gas, the solution is obtained by mapping the system onto a gas of non-interacting fermions subjected to the same external potential [30], $\Psi_{\text{TG}}(x_1, \dots, x_N) = \prod_{1 \leq j < \ell \leq N} \text{sgn}(x_j - x_\ell) \det[\psi_j(x_k)]$, with corresponding energy $E_{\text{TG}} = \sum_{k=0}^{N-1} \varepsilon_k$ and density profile $n(x) = \sum_{k=0}^{N-1} |\psi_k|^2$. The corresponding profile, illustrated in Fig. 2(c) displays typical Friedel oscillations [31].

Using the thermodynamic relation (1), we readily compute the persistent current and its amplitude [32], as illustrated in Fig. 3. We find that α is always larger in the TG regime than in the non-interacting one, both in the smeared-sawtooth and in the sinusoidal regime of current response. This behavior is explained noticing that the barrier suppresses the dependence on the Coriolis flux more strongly for the lowest-lying energy levels than for the high-energy ones [33]. As a result, α is smaller for non-interacting bosons occupying the lowest level ε_0 only than for the TG regime where the levels are filled up to the Fermi energy ε_N .

We proceed by exploring how these two limiting regimes of interaction strength are connected.

Weak interactions.—At weak interparticle interactions we can neglect the effects of the quantum fluctuations [34] and describe the fluid as a Bose-Einstein condensate making use of the mean-field GP equation, which in the co-rotating frame takes the form

$$\frac{\hbar^2}{2M} \left(-i \frac{\partial}{\partial x} + \frac{2\pi}{L}\Omega \right)^2 \Phi + U_0\delta(x)\Phi + g|\Phi|^2\Phi = \mu\Phi. \quad (3)$$

Here Φ is the condensate wavefunction and μ is the chemical potential. We have found an analytical soliton-like solution for Φ in terms of Jacobi elliptic functions [32], thus extending [35, 36] (see also [37–39] for related work). In particular, by comparing with the numerical solution of the GP equation, we find that the barrier pins the soliton and turns it to the ground-state solution. The resulting density profile is characterized by a minimum at the barrier position whose depth depends on the interaction strength, the barrier height, and the rotation velocity (see Fig. 2(a) and [32]). The corresponding en-

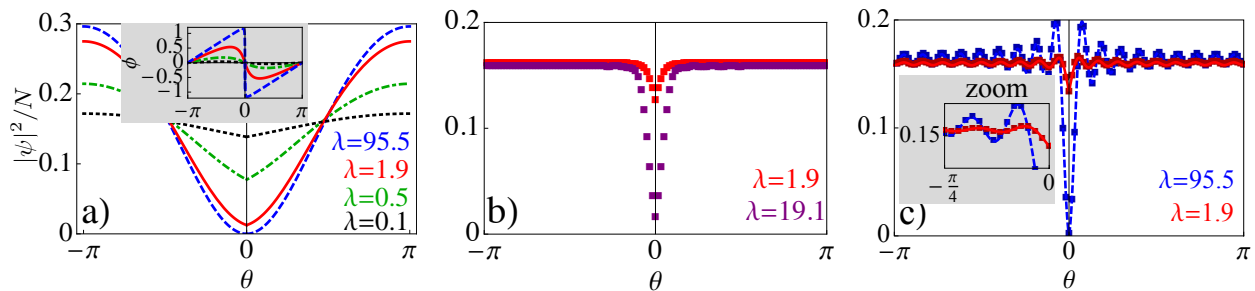


FIG. 2. (Color online). Density profiles vs angular coordinate θ along the ring at various values of the barrier strength λ , for (a) the GP soliton solution at weak interaction strength $\gamma = 0.01$ (the inset shows the soliton phase vs θ at the same values of barrier strength), (b) the MPS solution at intermediate interaction $\gamma = 3.3$, (c) the analytical TG solution (lines) vs. MPS (squares) in the hard-core limit. The parameters used are $N = 18$, $\Omega = 0.4$ in all the curves.

ergy is obtained from the GP energy functional $E_{\text{GP}}[\Phi] = \int dx \Phi^* (i\hbar\partial_x - Mv)^2 \Phi / 2M + g|\Phi|^4 / 2 + U_0\delta(x)|\Phi|^2$, which encodes the dependence on Ω in the condensate wavefunction. Using this approach, we find that the persistent current amplitude α at weak coupling increases monotonically with the interaction strength γ , as illustrated in Fig. 3. In this classical-field regime, the mean-field interaction term acts as an effective potential which screens the barrier potential, in a similar fashion as in a disordered system.

Strong interactions.—The LL theory [40, 41] is a low-energy, quantum hydrodynamics description of the bosonic fluid, in terms of the canonically-conjugate fields θ and ϕ corresponding to the density fluctuations and to the phase of the superfluid, respectively. This approach allows us to account for the interplay of barrier and quantum fluctuation effects on the persistent currents at strong interparticle interactions, up to the TG limit.

In the rotating frame, the effective low-energy LL Hamiltonian for a uniform ring is

$$\mathcal{H}_0 = \frac{\hbar v_s}{2\pi} \int_0^L dx \left[K \left(\partial_x \phi(x) - \frac{2\pi}{L} \Omega \right)^2 + \frac{1}{K} (\partial_x \theta(x))^2 \right]. \quad (4)$$

Details of the microscopic interactions enter through the Luttinger parameter K and the sound velocity v_s . In the case of repulsive contact interactions their dependence on the interaction strength is known (see, *e.g.*, Ref. [42]): at vanishing interactions, K tends to infinity and v_s vanishes, while, in the TG limit, $K = 1$ and v_s corresponds to the Fermi velocity of the fermionized Bose gas.

We first analyze perturbatively the regime of *weak barrier strength*. The barrier contribution to the Hamiltonian $\mathcal{H}_b = \int dx U_0 \delta(x) \rho(x)$ is obtained by keeping only the lowest harmonics in the density field expansion $\rho(x) = [n_0 + \partial_x \theta(x) / \pi] \sum_{l=-\infty}^{+\infty} e^{2il\theta(x) + 2il\pi n_0 x}$, yielding as most important term $\mathcal{H}_b \sim 2U_0 n_0 \cos[2\theta(0)]$. This backscattering term breaks angular momentum conservation, allowing for jumps by one unit of angular momentum $J \rightarrow J \pm 1$. By integrating out the density-

fluctuation modes in the barrier Hamiltonian, we obtain a renormalized barrier strength $U_{\text{eff}} = U_0 (d/L)^K$, where d is a suitably-chosen short-distance cut-off [32]. The final result for the persistent current close to the frustration point $\Omega = 1/2$ is

$$I(\Omega)/N = -I_0 \delta\Omega \left[1 - \left(2\sqrt{\delta\Omega^2 + \lambda_{\text{eff}}^2} \right)^{-1} \right], \quad (5)$$

where $\delta\Omega = \Omega - 1/2$, $\lambda_{\text{eff}} = MU_{\text{eff}}L/2\pi^2\hbar^2$ and $I_0 = 2\pi\hbar/M L$. The corresponding amplitude is illustrated in Fig. 3. For decreasing interactions down from the TG limit, α increases: the effective barrier decreases due to the effect of quantum fluctuations.

In the opposite case of *strong barrier strength*, we model the transport across the barrier with a tunneling Hamiltonian $\mathcal{H}_t = 2tn_0 \cos[\phi(L) - \phi(0) + 2\pi\Omega]$, where t is the tunneling amplitude. By averaging out the quantum phase fluctuations in the tunnel Hamiltonian \mathcal{H}_t , we obtain a renormalization of the tunnel amplitude [43], *i.e.*

$$I(\Omega)/N = -(t/\pi\hbar)(d/L)^{1/K} \sin(2\pi\Omega). \quad (6)$$

The link between the tunnel amplitude and the barrier height is obtained by making use of duality between the models describing the weak and the strong barrier limits [32, 44].

Both for weak and large barrier, the Luttinger description on a mesoscopic ring is expected to break down for sufficiently weak interactions when the short-distance cutoff required in the theory increases, until it becomes comparable with the system size.

The persistent current amplitude in the case of large barrier is also shown in Fig. 3. Interestingly, the renormalization of the barrier at intermediate interaction is so effective to turn a relatively large barrier into a weak one. This completely changes the physical scenario and illustrates the dramatic effect of interplay of interactions and quantum fluctuations.

Intermediate interactions and barrier strengths.— Away from the weakly and the strongly interacting regime, and for arbitrary barrier strength it is difficult to

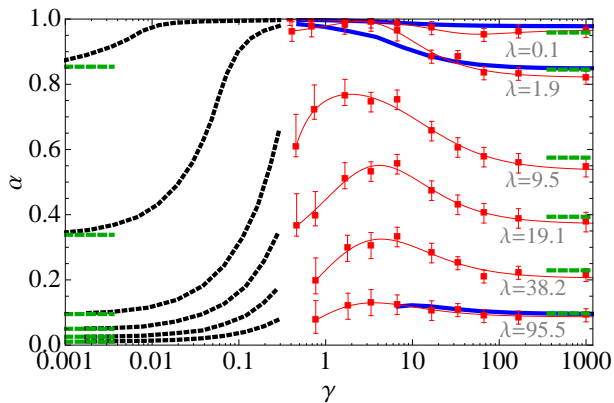


FIG. 3. (Color online) Persistent current amplitude α (dimensionless quantity) as a function of the dimensionless interaction strength γ for $N = 18$ and various values of the barrier strength as indicated in the figure, according to the mean-field GP equation (black dotted lines), the Luttinger-liquid small- and large-barrier predictions (blue solid lines), the numerical MPS calculations (red squares, red thin solid lines are guides to the eye) and ideal gas and TG exact solutions (green dashed lines).

tackle the many-body Schrödinger equation corresponding to Hamiltonian (2) with analytical approaches, and we employ numerical simulations based on the density-matrix renormalization-group (DMRG) approach to explore this regime. After discretizing the space and mapping Hamiltonian (2) onto a Bose-Hubbard model on a 1D lattice with periodic boundary conditions [32], we represent its corresponding ground-state wavefunction $\Psi_{\text{lat}}(x_1, \dots, x_N)$ as a MPS. We then perform a variational minimization of the energy cost function site by site. In order to recover the continuum limit, we keep the on-site bosonic occupation $\langle n_j \rangle \lesssim 0.15$. Special care has to be taken with periodic boundaries, which are intrinsically more difficult to be handled with DMRG-like approaches. In our case, we introduced a factorization procedure for long products of MPS matrices, which reduces the computational effort [32, 45].

The resulting density profiles are shown in Fig. 2. At large interactions they display Friedel oscillations, which are instead strongly damped at intermediate interactions. We find very good agreement with the analytical predictions in the TG limit.

As illustrated in Fig. 3, our MPS method also gives us the possibility to obtain the amplitude of the persistent current α for a large range of barrier heights λ and interaction strengths γ [46]. We find a non-monotonous behavior which connects the weak- and strong-interaction results. This allows to confirm the expected regimes of validity of the analytical estimates. We also note that the position of the maximum, *i.e.*, the optimum persistent current depends on the barrier strength.

Conclusions.—Our main results are summarized in

Fig. 3. In a one-dimensional ring with a localized barrier, the persistent current amplitude is a non monotonous function of the interaction strength and displays a pronounced maximum as a function of the interaction strength, in all regimes of barrier strength. The maximum is due to the fact that, while at increasing interactions a classical bosonic field screens more and more the barrier, going towards the strongly correlated Tonks-Girardeau regime quantum fluctuations screen less and less the barrier, due to the increasingly fast spatial decay of phase-phase correlations [47]. Our results imply that, in a large range of interaction strengths, unwanted impurities or imperfections on the ring are expected to only weakly affect the system properties. On the other hand, for the applications to quantum state manipulation, the regimes of choice should be either very weak or very strong interactions, since these are the regimes where the system responds stronger to a localized external probe. Our analysis can be readily extended to include temperature effects and thermal fluctuations [17, 19, 48, 49]: they give rise to additional smearing of the persistent current shape starting from a typical temperature $k_B T \sim N E_0 = 2\pi^2 \hbar^2 n_0 / ML$. Taking into account typical experimental constraints on energy and time scales, persistent currents might be observed in the next-generation experiments of mesoscopic ring traps on a chip (*i.e.*, with a ring diameter of $\sim 5 \mu\text{m}$, corresponding to a typical energy $N E_0 \sim 550 \text{ Hz}$ for ^{87}Rb atoms taking $N = 18$). Our results are also relevant to other mesoscopic bosonic quantum fluids, as thin superconducting rings and solid-state photonic or polaritonic nanocavities etched on a ring-necklace shape.

We are indebted to L. Amico, R. Citro, R. Fazio, L. Glazman, I. Safi, P. Silvi and W. Zwerger for useful discussions. This work is supported by the ERC Handy-Q grant N.258608, by Institut universitaire de France and by Italian MIUR through FIRB Project No. RBFR12NLNA. MPS simulations were performed on the TQO cluster of the Max-Planck-Institut für Quantenoptik (Garching) and on MOGON cluster in Mainz.

Supplemental Material for: “Optimal persistent currents for ultracold bosons stirred on a ring”

Details of the exact solutions for the limiting cases of ideal and Tonks-Girardeau gas

We outline the solution for the single particle problem used to obtain the ideal-gas and the Tonks-Girardeau (TG) solution of the main text. The single particle eigenfunctions of the one-body Schrödinger equation take the form

$$\psi_n(x; \Omega) = \begin{cases} \frac{1}{\mathcal{N}_n} e^{-i\Omega\pi} [e^{ik_n(x-L/2)} + A_{n,\Omega} e^{-ik_n(x-L/2)}] & x \in [0, L/2) \\ \frac{1}{\mathcal{N}_n} e^{i\Omega\pi} [e^{ik_n(x+L/2)} + A_{n,\Omega} e^{-ik_n(x+L/2)}] & x \in [-L/2, 0) \end{cases} \quad (7)$$

By imposing twisted boundary conditions, unity normalization and the cusp condition $\partial_x \psi_n^+(0^+; \Omega) - \partial_x \psi_n^-(0^-; \Omega) = \lambda \psi_n(0; \Omega)$, we obtain

$$k_n = \pm \lambda \frac{\pi}{L} \frac{\sin(k_n L)}{\cos(2\pi\Omega) \mp \cos(k_n L)},$$

where the \pm sign refers to a number of particles N odd or even respectively [53], $A_{n,\Omega} = \frac{\sin(k_n L/2 + \Omega\pi)}{\sin(k_n L/2 - \Omega\pi)}$ for N odd and $A_{n,\Omega} = -\frac{\cos(k_n L/2 + \Omega\pi)}{\cos(k_n L/2 - \Omega\pi)}$ for N even, while $\mathcal{N}_n = \sqrt{L \left(1 + A_{n,\Omega}^2 + 2A_{n,\Omega} \frac{\sin(k_n L)}{k_n L} \right)}$ is the normalization factor.

Weak barrier limit — In the regime $\lambda \ll 1$ we determined perturbatively the persistent current amplitude, choosing for simplicity N odd. The single-particle energy levels are obtained by degenerate perturbation theory around the unperturbed parabolas $\varepsilon_n = \frac{(2\pi\hbar)^2}{2ML^2} (\Omega - n)^2$. Close to the frustration point $\Omega = 1/2$ the pairs of degenerate levels are ε_n and ε_{1-n} . We immediately get

$$\varepsilon_n^{(\pm)} = \frac{(2\pi\hbar)^2}{2ML^2} \left\{ [\delta\Omega^2 + (n - 1/2)^2] \pm 2(n - 1/2) \sqrt{\delta\Omega^2 + \tilde{\lambda}_n^2} \right\} \quad (8)$$

where $\delta\Omega = \Omega - 1/2$ and $\tilde{\lambda}_n = \lambda/(2n - 1)$. The TG ground-state energy is given by $E_{\text{TG}} = \sum_{n=0}^{(N-1)/2} (\varepsilon_n^{(+)} + \varepsilon_n^{(-)})$. In this sum the \pm terms in the r.h.s. of Eq. (8) compensate except the highest-energy one [54], yielding Eq. (5) of the main text with $\lambda_{\text{eff}} \simeq \lambda/N$. This allows us to choose the short-distance cutoff of the Luttinger theory (see below).

Details of the soliton-like solution at weak interactions

We discuss the soliton-like solution of the GP equation, Eq. (3) in the main text. Our approach extends the one of Ref. [35] to the case where a delta barrier is present. We first recast the GP equation in dimensionless form by introducing $\tilde{\Phi}(\theta) = \sqrt{L/2\pi} \Phi(2\pi x/L)$, $\tilde{\mu} = ML^2 \mu / (2\pi^2 \hbar^2)$ and $\tilde{g} = gMNL / (\pi \hbar^2)$, and take $\theta \in [0, 2\pi]$. A parametrization of the condensate wavefunction in density-phase representation $\tilde{\Phi}(\theta) = f(\theta) e^{i\phi(\theta)}$ yields

$$-f'' + f(\phi')^2 - 2\Omega f\phi' + (\Omega^2 - \tilde{\mu} + \tilde{g}f^2)f = 0, \quad (9)$$

$$-2f'\phi' - f\phi'' + 2\Omega f' = 0. \quad (10)$$

The effect of the delta barrier is replaced by the cusp condition $f'(0^+) - f'(0^-) = \lambda f(0)$, where $\lambda = MU_0 L / (\pi \hbar^2)$, which, assuming a symmetric cusp $f'(0^+) = -f'(0^-)$ and introducing the density $s = f^2$ reads $s'(0^+) = \lambda s(0)$. We first integrate Eq. (10) to obtain ϕ' ,

$$\phi' = \frac{C}{f^2} + \Omega, \quad (11)$$

where C is an integration constant. Substituting this result into Eq. (9) we get $-f'' + C^2/f^3 + (\tilde{g}f^2 - \tilde{\mu})f = 0$, which, upon integration and change of variables, yields

$$s'^2 = -4C^2 + 2\tilde{g}s^3 - 4\tilde{\mu}s^2 + 4As,$$

A being an integration constant. Introducing the potential $U(s) = 2C^2 - 2As + 2\tilde{\mu}s^2 - \tilde{g}s^3$, we see that the problem is equivalent to the one of a classical particle of unitary mass with position s and velocity s' having zero total energy. Denoting $U(s) = -\tilde{g}(s - s_1)(s - s_2)(s - s_3) = 0$ with $s_1 \leq s_2 \leq s_3$, an allowed trajectory is possible in the interval $s_1 < s < s_2$ if $A > 0$. In the presence of the barrier, in order to satisfy the cusp condition, the soliton trajectory starts at initial position $s_{\min} > s_1$. The soliton is then found upon integration,

$$\int_{s_{\min}}^{s(\theta)} \frac{ds'}{\sqrt{-2U(s')}} = \int_0^\theta d\theta' = \theta$$

Introducing the change of variable $y^2 = (s - s_1)/(s_2 - s_1)$, the integral corresponds to the Jacobi elliptic function $\text{sn}(u|m)$ with $m = (s_2 - s_1)/(s_3 - s_1)$. By imposing periodic boundary conditions for the condensate density (*i.e.*, requiring that at half-period the soliton solution reaches its maximum value $s = s_2$), we find $\pi\sqrt{\tilde{g}(s_3 - s_1)/2} + \alpha = K$ and

$$s(\theta) = s_1 + (s_2 - s_1)\text{sn}^2[(K - \alpha)\theta/\pi + \alpha]. \quad (12)$$

Here $\alpha = F[\arcsin(\sqrt{(s_{\min} - s_1)/(s_2 - s_1)})|m]$ with $F[\phi|m]$ being the incomplete elliptic integral of the first kind, and K is the corresponding complete elliptic integral.

Imposing the normalization condition $\int_0^{2\pi} d\theta s(\theta) = 1$ we obtain

$$2\pi s_1 + 4(K - \alpha)(K - \alpha - E + \alpha')/(\pi\tilde{g}) = 1,$$

where $E[\phi|m]$ and E are respectively the incomplete and complete elliptic integrals of the second kind, and $\alpha' = E[\arcsin(\sqrt{(s_{\min} - s_1)/(s_2 - s_1)})|m]$. Substituting Eq. (12) for s in equation $s'^2 = -2U(s)$ and equating the terms with the same power of sn , yields the following parameter identification:

$$\tilde{\mu} = 3\tilde{g}s_1/2 + (1 + m)[(K - \alpha)/\pi]^2; \quad (13)$$

$$A = 2\tilde{\mu}s_1 - 3\tilde{g}s_1^2/2 - 2m[(K - \alpha)/\pi]^4/\tilde{g}; \quad (14)$$

$$C^2 = As_1 - \tilde{\mu}s_1^2 + \tilde{g}s_1^3/2. \quad (15)$$

Finally, the cusp condition yields an equation for s_{\min} ,

$$\lambda s_{\min} = \sqrt{-2U(s_{\min})}. \quad (16)$$

Equations (13 – 16) form a coupled set of equations which can be solved as a function of m and s_{\min} .

Using Eqs. (11) and (12), we then obtain the solution for the phase of the soliton solution:

$$\phi(\theta) = C(\Pi[(s_1 - s_2)/s_1; (K - \alpha)\theta/\pi + K|m] - \Pi[(s_1 - s_2)/s_1; \alpha|m])/(K - \alpha)s_1 + \Omega(\theta + \pi), \quad (17)$$

where $\Pi[n; u|m]$ is the incomplete elliptic integral of the third kind.

Imposing 2π -periodicity of the condensate wave function, integration of Eq. (11) yields $2\pi n = \int_{-\pi}^{\pi} d\theta \frac{C}{s} + 2\pi\Omega$, hence

$$2\pi(n - \Omega)/C = 2\pi(\Pi[(s_1 - s_2)/s_1; K|m] - \Pi[(s_1 - s_2)/s_1; \alpha|m])/((K - \alpha)s_1). \quad (18)$$

Fig. 4 shows the soliton density and phase at fixed barrier strength at varying Coriolis flux Ω , both for the $n = 0$ case of no winding, and of one quantum of angular momentum, *i.e.* $n = 1$.

In summary, we find the soliton solution according to the following strategy: for given values of the interaction constant \tilde{g} , the barrier strength λ and the Coriolis flux Ω , we express s_1 , s_2 and s_3 (hence $\tilde{\mu}$, A , and C) as a function of m and s_{\min} , then solve simultaneously Eq. (16) and the one obtained after equating Eqs. (18) and (15). This uniquely fixes m and s_{\min} , and hence the entire soliton solution.

By performing imaginary-time numerical integration of the GP equation, we have checked that the analytical soliton solution given by Eqs. (12), (17) coincides with the numerical ground state, see again Fig. 4.

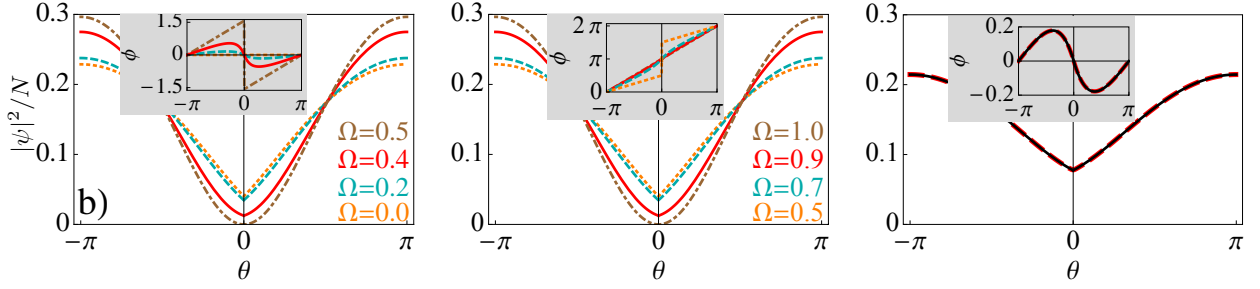


FIG. 4. Left and central panel, soliton solution for the density (main figure) and phase (inset) as a function of the spatial coordinate along the ring for various values of the reduced Coriolis flux Ω as indicated in each figure, at fixed dimensionless barrier height $\lambda = 1.9$, $N = 18$ and $\tilde{g} = 1$. Right panel, comparison of the analytical soliton solution of the GP equation (black solid line), with the numerical solution obtained via imaginary-time integration (red dashed line) taking $N = 18$, $\Omega = 0.4$, $\lambda = 0.5$, and $\tilde{g} = 1$. The numerical ground state energy in units of $2\pi^2\hbar^2/ML^2$ is $\tilde{E}_{\text{GS}}^{\text{num}} = 0.2965(3)$ to be compared with the one of the soliton solution $\tilde{E}_{\text{GS}}^{\text{sol}} = 0.2966$.

Details of the Luttinger-liquid solution

We outline the derivation yielding Eqs.(5) and (6) of the main text.

In the weak barrier case, we start from the mode expansion for the density and phase fields for the uniform ring,

$$\theta(x) = \theta_0 + \frac{1}{2} \sum_{q \neq 0} \left| \frac{2\pi K}{qL} \right|^{1/2} [e^{iqx} b_q + e^{-iqx} b_q^\dagger], \quad (19)$$

$$\phi(x) = \phi_0 + \frac{2\pi x}{L} (J - \Omega) + \frac{1}{2} \sum_{q \neq 0} \left| \frac{2\pi}{qLK} \right|^{1/2} \text{sgn}(q) [e^{iqx} b_q + e^{-iqx} b_q^\dagger], \quad (20)$$

where $q = 2\pi j/L$ with j integer, J is the angular momentum operator, K is here the Luttinger parameter and the following commutation relations hold: $[b_q, b_{q'}^\dagger] = \delta_{q,q'}$; $[J, e^{-2i\theta_0}] = e^{-2i\theta_0}$. The latter property implies that the zero-mode θ_0 acts as a (normalized) raising operator for the states $|J\rangle$ of given angular momentum: $e^{-2i\theta_0}|J\rangle = |J+1\rangle$.

The lowest-order relevant term in the barrier Hamiltonian induces transitions of one quantum of angular momentum [55] due to the zero-mode part in $\theta(x) \equiv \theta_0 + \delta\theta(x)$, *i.e.*

$$\mathcal{H}_b \sim 2U_0 n_0 \cos(2\theta(0)) = n_0 U_0 \sum_J |J-1\rangle \langle J| e^{2i\delta\theta(0)} + |J\rangle \langle J+1| e^{-2i\delta\theta(0)}.$$

The calculation is performed in two steps. First, using the mode expansion of the fields and averaging the total Hamiltonian over the nonzero modes, we obtain an effective Hamiltonian for the angular momentum operator [56]

$$\mathcal{H}_J = E_0 (J - \Omega)^2 + n_0 U_{\text{eff}} \sum_J |J+1\rangle \langle J| + \text{H.c.} \quad (21)$$

The effective barrier strength U_{eff} is obtained by averaging over the phase fluctuations $U_{\text{eff}} = U_0 \langle e^{\pm i2\delta\theta(0)} \rangle = U_0 (d/L)^K$, d being a short-distance cutoff of the order of the interparticle distance. By choosing $d = K/n_0$, this expression coincides with the exact TG result at $K = 1$ (see above) and takes into account the shrinking of the linear region of the excitation spectrum once interactions are decreased away from the TG point.

In a second step, we perform degenerate perturbation theory between states of given angular momentum, obtaining $E(\Omega)/N = E_0 [\delta\Omega^2 - \sqrt{\delta\Omega^2 + \lambda_{\text{eff}}^2}]$, with $E_0 = 2\pi^2\hbar^2/ML^2$, $\delta\Omega = \Omega - J - 1/2$, and $\lambda_{\text{eff}} = MU_{\text{eff}}L/2\pi^2\hbar^2$. Upon using the thermodynamic relation (1) of the main text one readily obtains Eq. (5) of the main text.

In the strong barrier or weak-tunnel limit the appropriate mode expansion is the one with open boundary conditions,

$$\theta(x) = \theta_0 + i \sum_{q>0} \left(\frac{\pi K}{qL} \right)^{1/2} \sin(qx) [b_q - b_q^\dagger], \quad (22)$$

$$\phi(x) = \phi_0 + \sum_{q>0} \left(\frac{\pi}{qLK} \right)^{1/2} \cos(qx) [b_q + b_q^\dagger], \quad (23)$$

where $q = j\pi/L$ with j integer. Note that no circulation is allowed in the limit of infinitely large barrier, and hence the angular momentum J does not enter here. As in the weak-barrier case, we average the barrier-contribution of the Hamiltonian over the fluctuation modes obtaining the Ω -dependent part of the energy, $E(\Omega)/N = -2(t/L)\langle\cos(\phi(L) - \phi(0) - 2\pi\Omega)\rangle = -2(t/L)(d/L)^{1/K} \cos(2\pi\Omega)$, where we have made the same choice for the short-distance cut-off length d as in the weak-barrier case above. This readily leads to Eq.(6) of the main text.

The relation between tunneling amplitude t and dimensionless barrier strength $\lambda = MU_0L/\pi\hbar^2$ at given interparticle interactions is obtained using the result [44],

$$t/L = \Gamma(1 + K) \Gamma(1 + 1/K)^K (\hbar\omega_c)^{1+K} (U_0L)^{-K}, \quad (24)$$

where the model-dependent cut-off frequency ω_c is determined using the exact TG result in the case $K = 1$. In essence, for large values of the barrier strength we perform exact calculations of the current I vs Coriolis flux Ω , then use Eq. (6) of the main text as fitting function to extract the value of the tunnel amplitude t . The resulting dependence of t on the barrier strength is shown in Fig. 5. For sufficiently large values of the barrier strength (*i.e.*, $\lambda \gtrsim 50$) a very good agreement is found with the hyperbolic law (24), allowing therefore to extract ω_c .

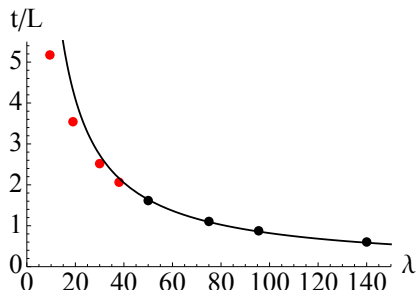


FIG. 5. Tunneling amplitude t vs. barrier strength λ in the TG limit for $N = 18$. For the red dots, the value of λ is too weak for the tunneling approximation to hold, and a deviation from the hyperbolic behavior is observed.

Details of the matrix-product-state numerical approach at intermediate interactions

In order to tackle the ground-state many-body problem for intermediate interactions, we resorted to numerical simulations based on a discretized version of the Hamiltonian (2) in the main text. This can be written in terms of the Bose-Hubbard model for a 1D chain of N_s lattice sites with periodic boundary conditions (PBC):

$$\mathcal{H}_{\text{lat}} = -t_{\text{BH}} \sum_{j=1}^{N_s} (e^{2\pi i\Omega/N_s} b_j^\dagger b_{j+1} + \text{H.c.}) + \frac{U_{\text{BH}}}{2} n_j(n_j - 1) - \mu_j n_j, \quad (25)$$

where b_j^\dagger (b_j) denote the creation (annihilation) operators of a boson in the second quantized form at site j , satisfying usual commutation relations. The real parameter t_{BH} denotes the amplitude of the hopping for bosons on adjacent sites, while its phase twist Ω/N_s is the net effect of a Coriolis flux Ω piercing the ring, within the standard Peierls construction. The on-site repulsion strength is denoted by U_{BH} . Finally $\mu_j \equiv \mu - \beta \delta_{j,1}$ is a chemical potential, which is uniform on all the sites but one, and sets the number of particles in the system in the grand canonical ensemble. The barrier is supposed to be localized on site $j = 1$, and has strength β .

By taking the continuum limit of Eq. (25), we link the parameters t_{BH} , U_{BH} and β of the Bose-Hubbard model to the parameters M , g and U_0 of the continuum Hamiltonian (2) in the main text. Specifically we have $\hbar^2/2M = t_{\text{BH}}a^2$, $g = U_{\text{BH}}a$ and $U_0 = a\beta$, where a is the lattice spacing of the discrete model.

Our numerical simulations are based on the Density Matrix Renormalization Group (DMRG) method, (see, *e.g.*, Ref. [57]). Specifically, we have used a Matrix Product State (MPS) representation of the many-body wavefunction and performed a variational minimization of the energy cost function, ruled by Eq. (25), site by site. We controlled the accuracy of the simulation by adjusting the size m of each matrix (bond link) composing the MPS. It is worth mentioning that special care has to be taken for PBC systems with a DMRG-based algorithm, since it performs a factor m^2 worse than for open-ended systems [58, 59]. Here we adopted an improved method based on the controlled

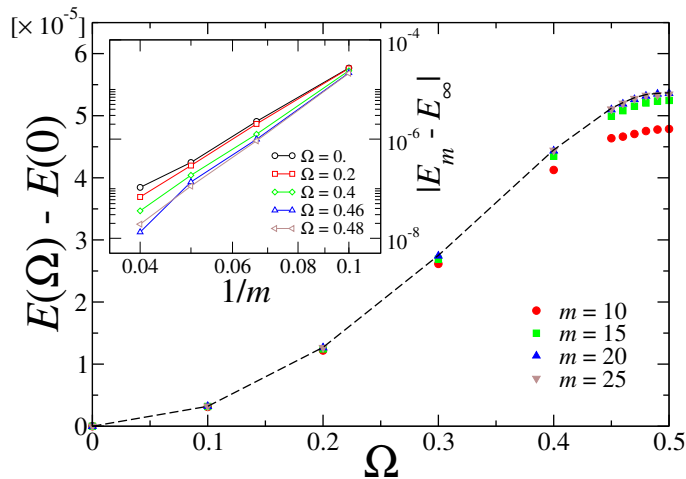


FIG. 6. Ground-state energy per lattice site, in units of t_{BH} , for the system described by the Hamiltonian in Eq. (25), as a function of the phase twist Ω and for different values of the bond-link dimension m (here we fixed $p = s = 4m$). The dashed line is obtained by extrapolating the values of the energies for $m \rightarrow \infty$, according to a power-law fit of the numerical data (symbols): $E_m \sim E_\infty + A m^{-B}$. Here we simulated a Bose-Hubbard chain of length $L = 120$, with $U_{\text{BH}} = 10$, $\mu = -1.81$, $\beta = 1$ (parameters are expressed in units of t_{BH}). We also chose $n_{\text{max}} = 2$, checking that this is sufficient with this value of interaction. Inset: Scaling of the energies with m , for fixed values of Ω .

factorization procedure for long products of MPS transfer matrices, which takes into account only $p \ll m^2$ singular values, without compromising the accuracy and reducing the computational effort [45, 60, 61]. This is justified by the fact that, for large chains, the local physics of the system is weakly affected by the properties of the boundaries. In a similar fashion, we approximated the effective Hamiltonian on the MPS basis by expanding it via a singular value decomposition, keeping only the contributions associated to its $s \sim p$ largest eigenvalues [45]. Furthermore we point out that the implementation of any symmetry in the variational MPS wavefunction, such as, in our case, the one accounting for the conservation of the total number of bosons, is less trivial with PBC rather than with OBC [62]. This forces us to work in the grand canonical ensemble and fix an average number of particles by suitably tuning the chemical potential.

We simulated Eq. (25) choosing $N_s = 120$ sites and fixing the chemical potential $\mu = \mu(t_{\text{BH}}, U_{\text{BH}})$ in such a way to have $N \sim 18$ particles in the system. A fine-tuning of μ in order to have a well defined number of particles has been performed in absence of any barrier, in the case when the system is translationally invariant (the effect of a finite β is that of smearing such accuracy in N —see below). We thus kept an average low filling $\langle n_j \rangle \lesssim 0.15$ (here $n_j = b_j^\dagger b_j$ counts the number of bosons on site j), mimicking the continuum limit of Eq.(2) of the main text and minimizing lattice effects. The simulations presented in Fig. (2) and Fig. (3) of the main text have been performed with $m = 20$, while we fixed $p = s$ up to 120. We also cut the maximum allowed occupation per site to n_{max} bosons, going from $n_{\text{max}} = 1$ in the TG regime, to $n_{\text{max}} = 4$ for $U_{\text{BH}} = 0.1$ (the lowest chosen value for U_{BH} , in units of t_{BH}).

We carefully checked that $m \simeq 20$ is already sufficient to get reliable results for the particle current $I(\Omega) \sim -\partial_\Omega E$, where $E(\Omega)$ is the ground-state energy. An example of the typical performances of our MPS code as varying the bond-link dimension m is provided in Fig. 6, where we explicitly show the dependence of the ground-state energy E as a function of the phase twist Ω . For fixed Ω , we found a dependence of such energy on m consistent with a power-law behavior: $E_m \sim E_\infty + A m^{-B}$, from which we could extrapolate the asymptotic value E_∞ (see the inset). We point out that the bond link values we considered for this work are considerably smaller than those used in typical DMRG simulations for open-ended chains, where $m_{\text{obc}} \sim 500$ could be easily reached. Nonetheless they are sufficient to reach an accuracy of the order 10^{-7} in terms of absolute values of energies, thus leading to an error in the extrapolation of the particle current $I(\Omega)$ of the order of 1%, that is barely visible on the scale of Fig. 6. A further and most important source of inaccuracies comes from the determination of the average number of particles N , which in some cases (especially for small interactions) becomes less accurate when varying the barrier strength. As a combination of these two sources of errors, the bars in Fig. 3 of the main text have been computed from point to point.

We found a very similar scenario for all the interaction regimes considered in this work.

-
- [1] B. S. Deaver and W. M. Fairbank, Phys. Rev. Lett., **7**, 43 (1961).
- [2] N. Byers and C. N. Yang, Phys. Rev. Lett., **7**, 46 (1961).
- [3] L. Onsager, Phys. Rev. Lett., **7**, 50 (1961).
- [4] L. P. Lévy, G. Dolan, J. Dunsmuir, and H. Bouchiat, Phys. Rev. Lett., **64**, 2074 (1990).
- [5] D. Mailly, C. Chapelier, and A. Benoit, Phys. Rev. Lett., **70**, 2020 (1993).
- [6] H. Bluhm, N. C. Koshnick, J. A. Bert, M. E. Huber, and K. A. Moler, Phys. Rev. Lett., **102**, 136802 (2009).
- [7] A. Bleszynski-Jayich, W. Shanks, B. Peaudecerf, E. Ginossar, F. von Oppen, L. Glazman, and J. Harris, Science, **326**, 272 (2009).
- [8] S. Gupta, K. W. Murch, K. L. Moore, T. P. Purdy, and D. M. Stamper-Kurn, Phys. Rev. Lett., **95**, 143201 (2005).
- [9] C. Ryu, M. F. Andersen, P. Cladé, V. Natarajan, K. Helmerson, and W. D. Phillips, Phys. Rev. Lett., **99**, 260401 (2007).
- [10] W. H. Heathcote, E. Nugent, B. T. Sheard, and C. J. Foot, New J. Phys., **10**, 043012 (2008).
- [11] K. Henderson, C. Ryu, C. MacCormick, and M. Boshier, New J. Phys., **11**, 043030 (2009).
- [12] B. E. Sherlock, M. Gildemeister, E. Owen, E. Nugent, and C. J. Foot, Phys. Rev. A, **83**, 043408 (2011).
- [13] A. Ramanathan, K. C. Wright, S. R. Muniz, M. Zelan, W. T. Hill, C. J. Lobb, K. Helmerson, W. D. Phillips, and G. K. Campbell, Phys. Rev. Lett., **106**, 130401 (2011).
- [14] S. Moulder, S. Beattie, R. P. Smith, N. Tammuz, and Z. Hadzibabic, Phys. Rev. A, **86**, 013629 (2012).
- [15] K. C. Wright, R. B. Blakestad, C. J. Lobb, W. D. Phillips, and G. K. Campbell, Phys. Rev. Lett., **110**, 025302 (2013).
- [16] L. Amico, D. Aghamalyan, H. Crepaz, F. Auzsotol, R. Dumke, and L.-C. Kwek, arXiv:1304.4615 (2013).
- [17] A. Zvyagin and I. Krive, Low. Temp. Phys., **21**, 533 (1995).
- [18] A. J. Leggett, “Granular Nanoelectronics,” (D.K.Ferry, J.R.Barker, and C.Jacoboni, Nato ASI Series B, 1991) p. 297.
- [19] D. Loss, Phys. Rev. Lett., **69**, 343 (1992).
- [20] A. Mueller-Groeling, H. Weidenmueller, and C. Lewenkopf, Europhys. Lett., **22**, 193 (1993).
- [21] B. S. Shastry and B. Sutherland, Phys. Rev. Lett., **65**, 243 (1990).
- [22] For a normal fluid on a ring the superfluid stiffness can be nonzero, however, it will vanish in the thermodynamic limit.
- [23] F. W. J. Hekking and L. I. Glazman, Phys. Rev. B, **55**, 6551 (1997).
- [24] K. A. Matveev, A. I. Larkin, and L. I. Glazman, Phys. Rev. Lett., **89**, 096802 (2002).
- [25] B. Paredes, A. Widera, V. Murg, O. Mandel, S. Fölling, I. Cirac, G. Shlyapnikov, T. Hansch, and I. Bloch, Nature, **429**, 277 (2004).
- [26] T. Kinoshita, T. Wenger, and D. Weiss, Science, **305**, 5687 (2004).
- [27] F. Bloch, Phys. Rev. B, **2**, 109 (1970).
- [28] F. Bloch, Phys. Rev. A, **7**, 2187 (1973).
- [29] E. H. Lieb and W. Liniger, Phys. Rev., **130**, 1605 (1963).
- [30] M. D. Girardeau, J. Mat. Phys., **1**, 516 (1960).
- [31] The Friedel oscillations weakly depend on the rotation velocity, as in [50].
- [32] See Supplemental Material for details.
- [33] C. Schenke, A. Minguzzi, and F. W. J. Hekking, Phys. Rev. A, **84**, 053636 (2011).
- [34] D. S. Petrov, G. V. Shlyapnikov, and J. T. M. Walraven, Phys. Rev. Lett., **85**, 3745 (2000).
- [35] R. Kanamoto, L. D. Carr, and M. Ueda, Phys. Rev. Lett., **100**, 060401 (2008).
- [36] R. Kanamoto, L. D. Carr, and M. Ueda, Phys. Rev. A, **79**, 063616 (2009).
- [37] M. Schechter, D. Gangardt, and A. Kamenev, Annals of Physics, **327**, 639 (2012), ISSN 0003-4916.
- [38] K. Anoshkin, Z. Wu, and E. Zaremba, Phys. Rev. A, **88**, 013609 (2013).
- [39] G. Arwas, A. Vardi, and D. Cohen, arXiv:1308.5860 (2013).
- [40] F. D. M. Haldane, Phys. Rev. Lett., **47**, 1840 (1981).
- [41] T. Giamarchi, “Quantum Physics in One Dimension,” (Oxford University Press, Oxford, 2004).
- [42] M. A. Cazalilla, Journal of Physics B: Atomic, Molecular and Optical Physics, **37**, S1 (2004).
- [43] Close to the TG limit, a renormalization group calculation yields corrections to the LL result, *i.e.*, an additional reduction of the tunnel energy [51].
- [44] U. Weiss, Solid State Communications, **100**, 281 (1996), ISSN 0038-1098.
- [45] D. Rossini, V. Giovannetti, and R. Fazio, J. Stat. Mech., P05021 (2011).
- [46] The MPS approach generally performs worse in the weakly interacting regime, where single-particle wavefunctions are delocalized across the lattice. Moreover the soft-core nature of bosons increases the inaccuracies due to the cutoff in the maximum on-site occupancy [32].
- [47] A non monotonous behaviour of tunnel current is also found in fermionic systems in the BCS-BEC crossover [52].
- [48] K. K. Das, M. D. Girardeau, and E. M. Wright, Phys. Rev. Lett., **89**, 170404 (2002).
- [49] P. Vignolo and A. Minguzzi, Phys. Rev. Lett., **110**, 020403 (2013).
- [50] W. Zwerger, L. Bönig, and K. Schönhammer, Phys. Rev. B, **43**, 6434 (1991).
- [51] D. Yue, L. I. Glazman, and K. A. Matveev, Phys. Rev. B, **49**, 1966 (1994).
- [52] A. Spuntarelli, P. Pieri, and G. C. Strinati, Phys. Rev. Lett., **99**, 040401 (2007).
- [53] This follows from the fact that the mapping function $\mathcal{A} = \prod_{1 \leq j < \ell \leq N} \text{sgn}(x_j - x_\ell)$ used to build the TG wavefunction $\Psi_{\text{TG}}(x_1, \dots, x_N) = \mathcal{A} \det[\psi_j(x_k)]$ is periodic (antiperiodic) for odd (even) N respectively; correspondingly, the single-particle orbitals need to be periodic (antiperiodic) for odd (even) N .

- [54] This is typical of fermionic systems, where only the highest occupied level determines the transport properties.
- [55] Higher harmonics in the expansion induce jumps of more than one unit of angular momentum, and this processes can be ignored in a weak barrier approximation.
- [56] A. O. Gogolin and N. V. Prokof'ev, *Phys. Rev. B*, **50**, 4921 (1994).
- [57] U. Schollwock, *Ann. Phys.*, **326**, 96 (2011).
- [58] F. Verstraete, D. Porras, and J. I. Cirac, *Phys. Rev. Lett.*, **93**, 227205 (2004).
- [59] F. Verstraete, V. Murg, and J. I. Cirac, *Adv. Phys.*, **57**, 143 (2008).
- [60] P. Pippian, S. R. White, and H. G. Evertz, *Phys. Rev. B*, **81**, 081103(R) (2010).
- [61] M. Weyrauch and M. V. Rakov, arXiv:1303.1333 (2013).
- [62] This study is presently under investigation, and will be subject to a future work by us.